Frequency-dependent seismic attenuation in the inner core
2. A scattering and fabric interpretation

Vernon F. Cormier and Xu Li[1]

Department of Geology and Geophysics, University of Connecticut, Storrs, Connecticut, USA

[1] Broadband velocity waveforms of PKIKP in the distance range 150–180° are inverted for a model of inner core attenuation due to forward scattering by a three-dimensional heterogeneous fabric. A mean velocity perturbation of $8.4 \pm 1.8\%$ and a scale length of heterogeneity of 9.8 ± 2.4 km are determined from 262 available PKIKP ray paths. The velocity perturbations are larger for polar than for equatorial paths, decrease with depth, and show anisotropy in both global and regional data. For paths beneath North America, the smallest scale lengths (1–5 km) tend to lie in either the upper 200 km of the inner core or along paths close to the rotational axis. The depth dependence of attenuation is roughly similar to that obtained assuming a viscoelastic origin, except a more abrupt transition is seen between higher attenuation in the upper inner core and lower attenuation in the lower inner core. This transition may be sharp enough to produce either a first- or second-order discontinuity with depth in the long-wavelength (composite) elastic moduli. A fabric that satisfies the observed depth dependence and anisotropy of attenuation requires solidification of iron crystals having high (>10%) intrinsic anisotropy, which are preferentially aligned in time and depth. Since weak velocity dispersion, elastic anisotropy, attenuation anisotropy, and their depth dependence agree with that predicted by such a fabric, we suggest that scattering attenuation is not a small fraction but, rather, the predominant mechanism of attenuation in the inner core in the 0.02–2-Hz frequency band. *INDEX TERMS:* 8115 Tectonophysics: Core processes (1507); 8124 Tectonophysics: Earth's interior—composition and state (8105); 7203 Seismology: Body wave propagation; 7207 Seismology: Core and mantle; 3210 Mathematical Geophysics: Modeling; *KEYWORDS:* inner core, seismic attenuation, scattering

1. Introduction

[2] The Earth is laterally heterogeneous everywhere and on every spatial scale, from the size of crystals or grains in rocks to the size of continents. Scattering will take place when seismic waves propagate in the heterogeneous Earth. Scattering attenuation occurs when energy that would have otherwise arrived at the time of the direct arrival is redistributed in space to other locations and in time to positions in the later coda following the direct arrival. By modeling the complexity of seismic waves, properties of the heterogeneities in the Earth can be estimated, including the distribution of scale lengths and the seismic impedance contrasts of heterogeneities. In a review, *Wu and Aki* [1988] concluded that the velocity perturbation in the crust and upper mantle varies from 0.1% to 10% and the scale length varies from 0.001 km to 1000 km.

[3] The general problem of scattering of elastic waves by heterogeneity within the Earth is a difficult one and analytical solutions are known for only a few special cases, and even in these instances the solutions are complicated and laborious to calculate. Thus, most seismological studies have employed various approximations in attempts to interpret scattered seismic waves. These include the assumptions of only one type of wave (acoustic approximation), low contrast in material properties (Born approximation), long wavelength with respect to scale length of heterogeneity (Rayleigh approximation), and short wavelength with respect to the scale length of the background medium (ray approximation). The differences between these approximations are discussed by *Korneev and Johnson* [1993a, 1993b, 1996], who compare the scattered waves predicted by these approximations with those predicted by analytical solutions for scattering by spherical inclusions.

[4] The domain of validity of either the "high frequency approximations" or "low frequency approximations" is frequently given in terms of the product of the wave number and scale length. For example, if the scale length a of scatterers is 0.1 km, the scattering of a P wave at 0.1 Hz and propagating at a velocity of 10 km/sec can be treated by a

---

[1]Now at Earth Resources Laboratory, Department of Earth, Atmospheric, and Planetary Science, Massachusetts Institute of Technology, Cambridge, Masschusetts, USA.

low frequency approximation ($ka \ll 1$, where k is wave number). If $a = 10$ km, the scattering of same P wave can be treated by the Mie approximation ($ka \sim 1$). Without a priori information on the distribution of scatterer size or shape, it is risky to assume a particular approximation. Thus, analytic solutions for scattering are preferred whenever they are computationally feasible. One possible analytic solution, which we considered in an earlier study [*Cormier et al.*, 1998], is a one-dimensional model consisting of thin layers. In the current study, we assume a three-dimensional distribution of scatterers in which the scatterers consist of spheres. Analytic solutions for scattering by single spheres have been given by *Korneev and Johnson* [1993a, 1993b, 1996], which *Kaelin and Johnson* [1998] have extended using a parabolic approximation to distributions of spheres to calculate an equivalent attenuating medium.

2. Modeling

2.1. Parameterization

[5] Based on *Korneev and Johnson*'s [1993a, 1993b, 1996] analytic solutions for scattering by a sphere, *Kaelin and Johnson* [1998] developed a general dynamic composite elastic medium (DYCEM) theory. DYCEM theory can be used with either non-self-consistent or self-consistent approximations to estimate velocity and attenuation of P- and S-waves at all frequencies for heterogeneous media with distributions of spherical inclusions. Except for large impedance contrasts, the results from the non-self-consistent method and the self-consistent methods differ little. Since the computational time for the non-self-consistent method is shorter, we use the non-self-consistent method to calculate the scattering operator.

[6] In the non-self-consistent method, the complex wave number of a P wave after traveling through the composite medium is given as

$$k = k_0 + \frac{3}{2k_0} \sum_{n=1}^{N} A_{n0} \frac{c_n}{R_n^3} \quad (1)$$

where k_0 is the wave number of the incident wave, N is the total number of different types of inclusions, R_n and c_n are the radius and concentration, respectively, of the nth type of inclusion with $\sum_{n=1}^{N} c_n = 1$. Here A_{n0} is the scattering function of the nth type of inclusion relative to a homogeneous type 0 background. Its formula was derived by *Korneev and Johnson* [1996] as

$$A_{n0} = \frac{i}{k_0} \sum_{l=0}^{\infty} (2l + 1) a_l^{pp} \quad (2)$$

Here a_l^{pp} is the lth-order canonical scattering coefficient for a P wave, which is a function of radius of the insclusion, wave numbers in the background matrix and inclusion, and the densities in the background matrix and inclusion. (For details, see Appendix A of *Korneev and Johnson* [1996].

[7] The complex wave number can be recast as a complex velocity and treated in the same way as in the viscoelastic inversion problem of paper 1 [*Li and Cormier*, 2002]. To simplify the inversion, two assumptions are taken in the three-dimensional scattering model for the inner core. Since large density contrasts across heterogeneities in the inner core are unlikely to dynamically persist, the densities of the inclusions and the background are assumed to be the same. Second, the percent perturbations of shear velocity and compressional velocity are assumed to be the same. Departure from this latter assumption will not affect estimates of scale length and only weakly affect the estimated magnitude of the P velocity perturbation. The model is thus described by two parameters: the P velocity perturbation and the scale length of scatterers (equivalent to the radius of the spherical inclusions). The velocities of inclusions are taken from a Gaussian distribution with the fixed mean velocity given by PREM and a varying perturbation. The concentration c_n is proportional to the probability density of the nth type of inclusion, which is just the Gaussian distribution function for velocity.

2.2. Pulse Attenuation and Velocity Dispersion

[8] Figures 1 and 2 show how the phase velocity and apparent Q^{-1} of this model varies with frequency for scale lengths varying from 0.1 to 51.2 km and velocity perturbation varying from 4.6% to 20%. The apparent Q^{-1} is estimated from

$$Q^{-1}(\omega) = 2 \, \text{Im}[\hat{\alpha}(\omega)]/\text{Re}[\hat{\alpha}(\omega)] = -2 \, \text{Im}[k(\omega)]/\text{Re}[k(\omega)] \quad (3)$$

where $k(\omega)$ is given in equation (1). Similar to viscoelasticity, a frequency band of peak attenuation will exist as will regions of both low and high dispersion. As the frequency approaches zero, the real part of the velocity and elastic modulus approaches the static limit predicted by theories for the elastic moduli of composite media [e.g., *Berryman*, 1980; *Kuster and Toksoz*, 1974]. At high frequencies, corresponding to wavelengths much smaller than the scale length of inclusions, it becomes increasingly possible to obtain a minimum time path solely confined to the highest velocity member of the composite. In this frequency band, velocity oscillates about a value closest to the member of the composite having the highest velocity. With increasing velocity perturbation, the magnitudes of attenuation and velocity dispersion increase. With increasing scale length, the peak in attenuation and region of strongest velocity dispersion are shifted to lower frequency. In contrast to the behavior of an absorption band of viscoelasticity, strong dispersion exists over a relatively narrow band of frequencies, being strongest in a narrow band just below the point where the attenuation achieves its peak. Figures 3a and 3b are the corresponding attenuation operators convolved with different incident wavelets. The effect of increasing the scale length and the velocity perturbation is to decrease the amplitudes and increase the duration of the output signals. Another significant effect is that with increasing scale length and velocity perturbation, the onset of the apparent first arrival is earlier.

2.3. Searching Ranges and Intervals

[9] For the scattering attenuation model, a possible searching range for velocity perturbation in the inner core is suggested by the elastic moduli predicted by *Stixrude and*
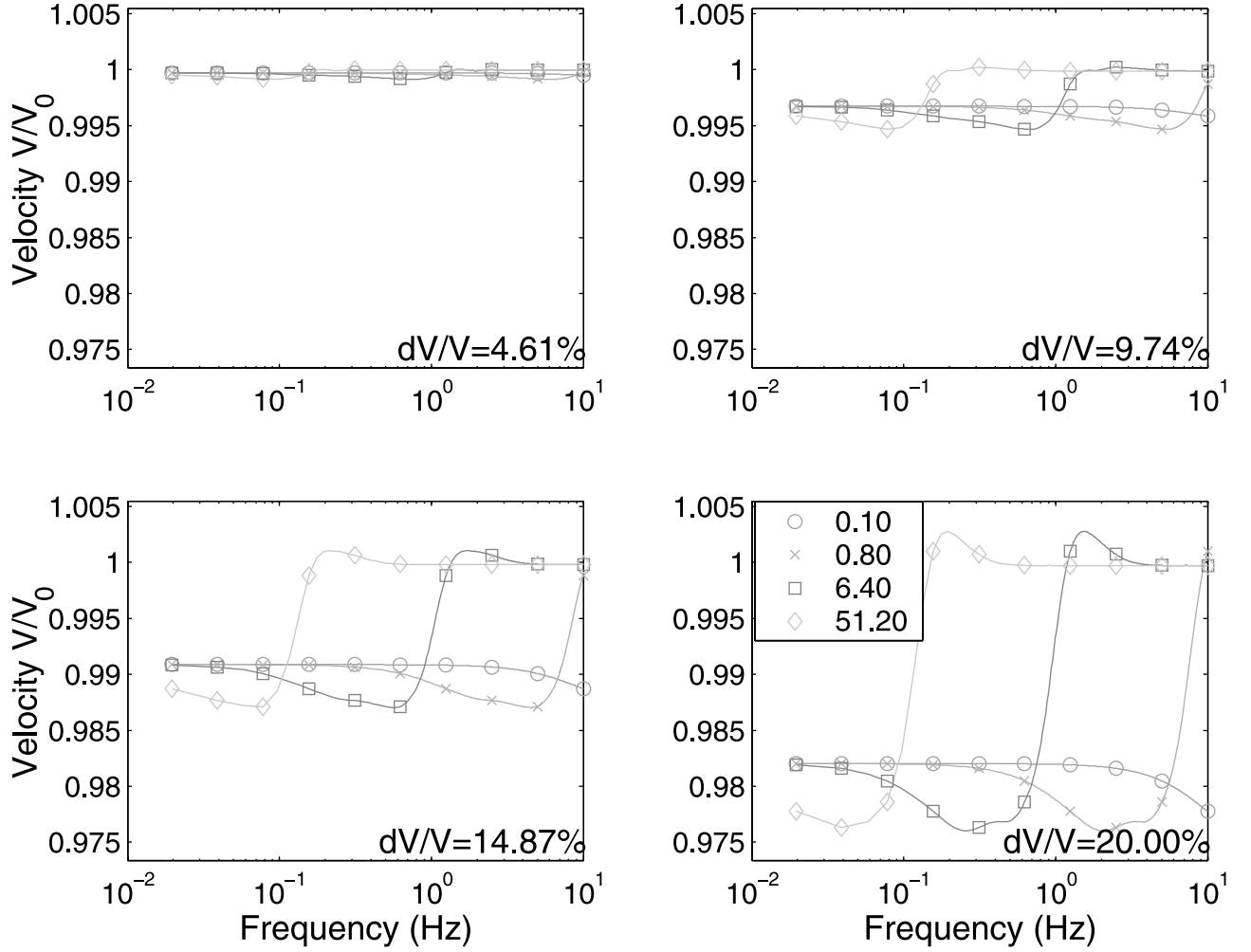
Figure 1. Velocity dispersion for a three-dimensional scattering model showing the dependence on scale length and velocity perturbation. The legend for scale length inset in the plot at the lower right is in units of km.

Cohen [1995] for hcp (hexagonal close-packed) and fcc (face-centered cubic) iron. The maximum difference in P wave velocity in different directions is about 4%. Recent first-principles calculations by *Steinle-Neumann et al.* [2001], however, predict much higher P wave velocity differences (12%) for hcp iron at inner core temperature and pressure. Allowing for this result and the possibility of heterogeneity in the form of inclusions of partial melt, the searching range for velocity perturbation was set as 0.5% to 20%.

[10] Both observational and theoretical constraints are also available for scale lengths of heterogeneity or sizes of anisotropic crystals in the inner core. Analysis of the coda of backscattered PKiKP coda by *Vidale and Earle* [2000] found a scale length of 2.5 km in the outer 300 km of the inner core. From extrapolation of laboratory experiments, *Bergman* [1998] suggested the scale length in the inner core varies from hundreds of meters to more than 10 km. Test inversions using upper bounds of 4 km and 8 km found that too many optimal fits to waveforms fell on the margins of the searching range, implying the upper bound

of 8 km may be too small. Hence, we chose a significantly higher upper bound of 51.2 km.

[11] Observed values of Q for seismic body wave in the inner core can provide another constraint for scale lengths. Figure 4 contours the apparent Q^{-1} at 1 Hz as a function of velocity perturbation and scale length. From this figure and assuming a range of Q^{-1} at 1 Hz of 0.001 to 0.02, we constrained the lower bound of scale length to 0.4 km. We note from Figure 4 that there can be two quite different values of scale length at each fixed value of velocity perturbation that produce the same apparent attenuation. This bimodal behavior of optimal solutions for a parameter is similar to the bimodal behavior of the low or high frequency relaxation time parameters of viscoelasticity discussed in paper 1. Unlike the ambiguity in the corner frequencies of viscoelasticity, however, we found that the ambiguity in predicted attenuation can sometimes resolved by the quite different dispersive properties of scattering versus viscoelasticity.

[12] The searching grid is equally spaced for velocity perturbation and spaced as a geometric series for scale
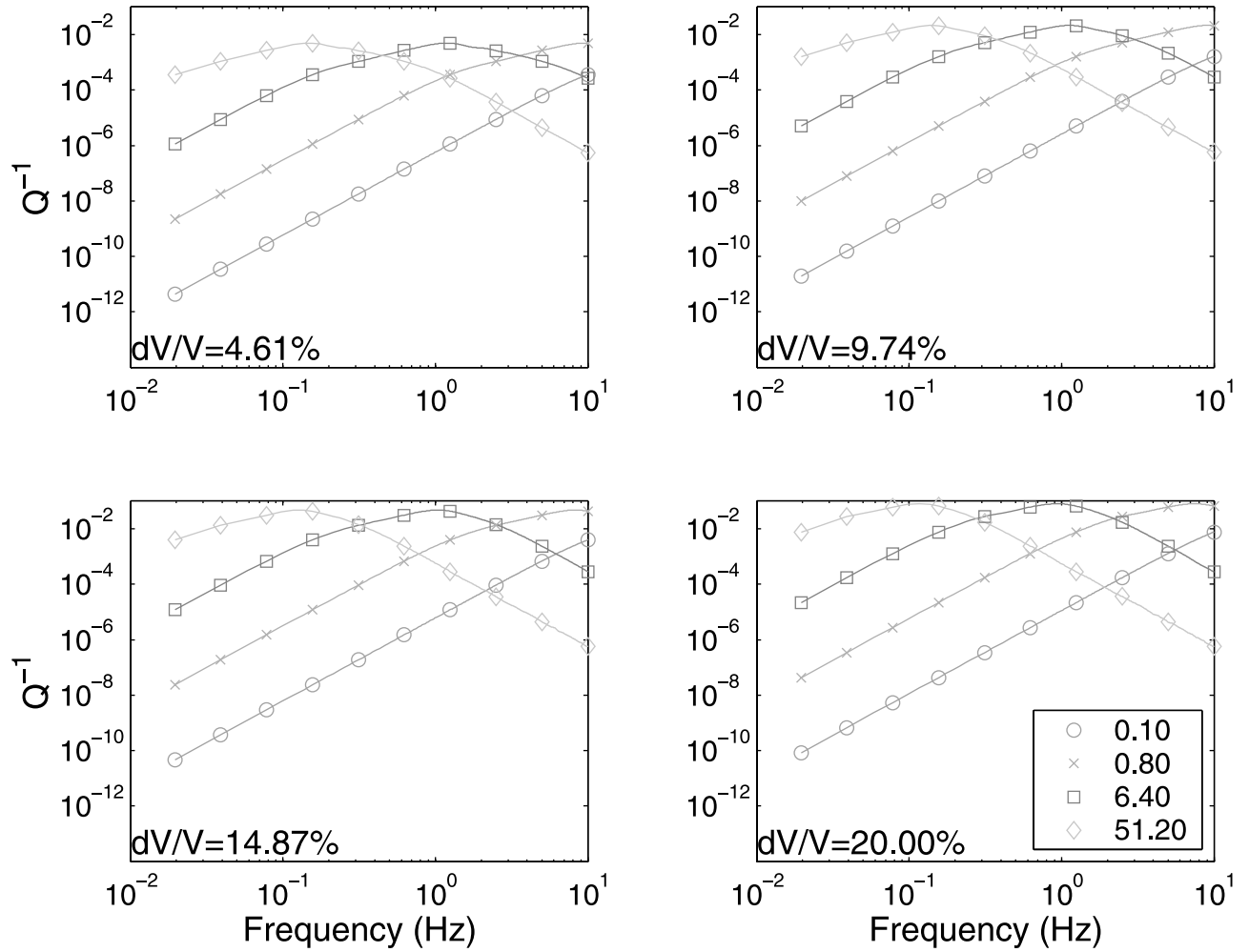
Figure 2. Apparent attenuation, Q^{-1}, in the seismic band for a three-dimensional scattering model showing dependence on scale length and velocity perturbation.

length (as in equation (5) of paper 1, but with x as scale length). Because it is time consuming to calculate the scattering attenuation operators, the probability density function for the an L_2 norm fit to waveforms is mapped

for only 10 discrete scale lengths and for 20 discrete velocity perturbations.

[13] Under North America, where the ray paths are relatively dense, a regional analysis can be performed. A regional
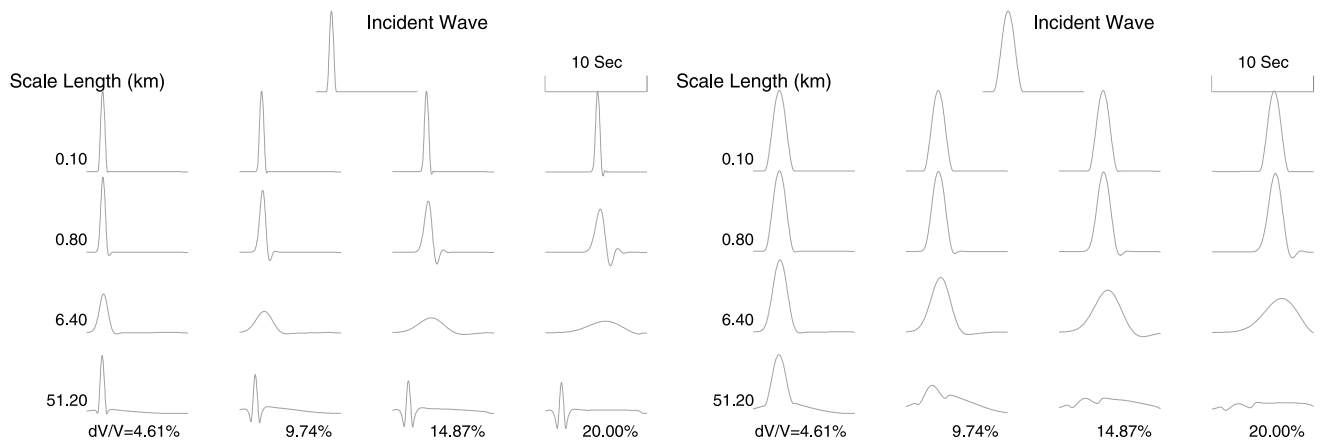

Figure 3. Forward scattering operators convolved with given wavelets. The travel distance is comparable to the diameter of the inner core. Amplitudes are normalized to that of the wavelet. (a) Wavelet has 1 s duration; (b) wavelet has 3 s duration.
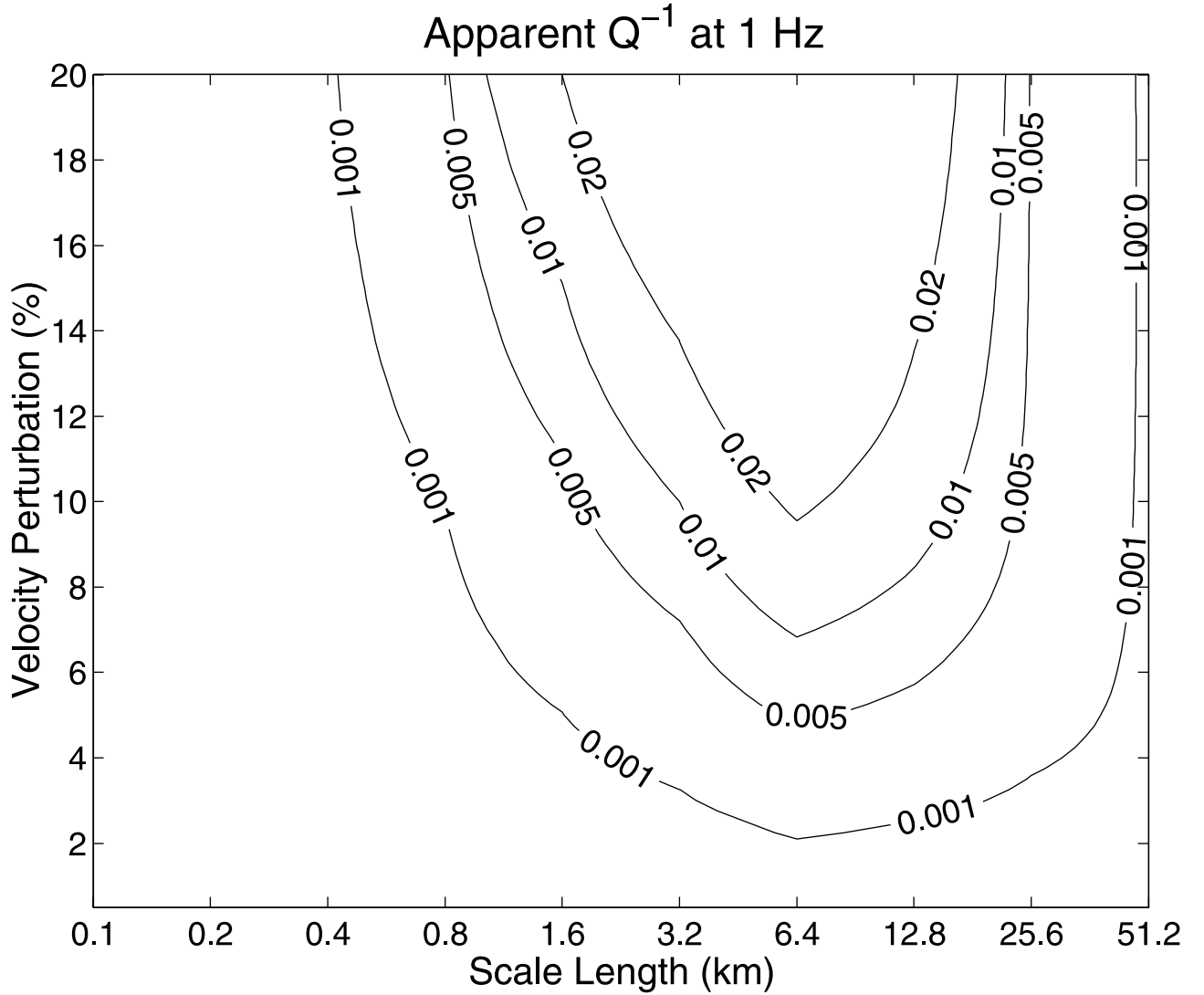
Apparent Q^{-1} at 1 Hz

Figure 4. Contours of apparent Q^{-1}(1 Hz) as a function of velocity perturbation and scale length in a three-dimensional scattering model. To model observed PKIKP pulse attenuation by scattering, a reasonable searching range for scale length of heterogeneity is estimated to be 0.4 km to several 10's of kms assuming a maximum P velocity perturbation of 20%.

analysis of scattering in the inner core beneath eastern Asia is not possible because of the fewer number of available ray paths.

3. Results

3.1. One-Dimensional Model

[14] In a previous study [*Cormier et al.*, 1998], waveforms were synthesized in a 1-D vertically varying medium, assuming a normally incident P wave, using a reflectivity approach as described by *Richards and Menke* [1983]. From our 1-D modeling, we suggested that the fabric needed to explain the observed attenuation completely by scattering may consist of disorder among either single or groups of ordered intrinsically anisotropic crystals. We concluded that such crystals must have P velocity differences of at least 5% and as much as 12% between two crystallographic axes at scale lengths of 0.5 to 2 km. The 1-D model layered medium

was chosen for modeling primarily because it was simple to compute, but it implicitly assumes an anisotropic distribution of scale lengths, in which the horizontal scale length is much larger than then the vertical scale length in the direction perpendicular to the Fresnel volume surrounding a PKIKP ray. Hence, one would like to check the validity of the 1-D estimates using a theory for 3-D heterogeneity having an isotropic distribution of scale lengths.

3.2. Three-Dimensional Model

[15] The attenuation operator for a 3-D scattering model can be obtained by using a non-self-consistent theory for complex wave number [*Kaelin and Johnson*, 1998], as described in section 2. The inverse method and postprocessing are similar to those for intrinsic attenuation, except rather than a corner frequency and attenuation at 1 Hz the two model parameters are scale length and velocity perturbation. The final results are given in Figures 5 and 6. Good
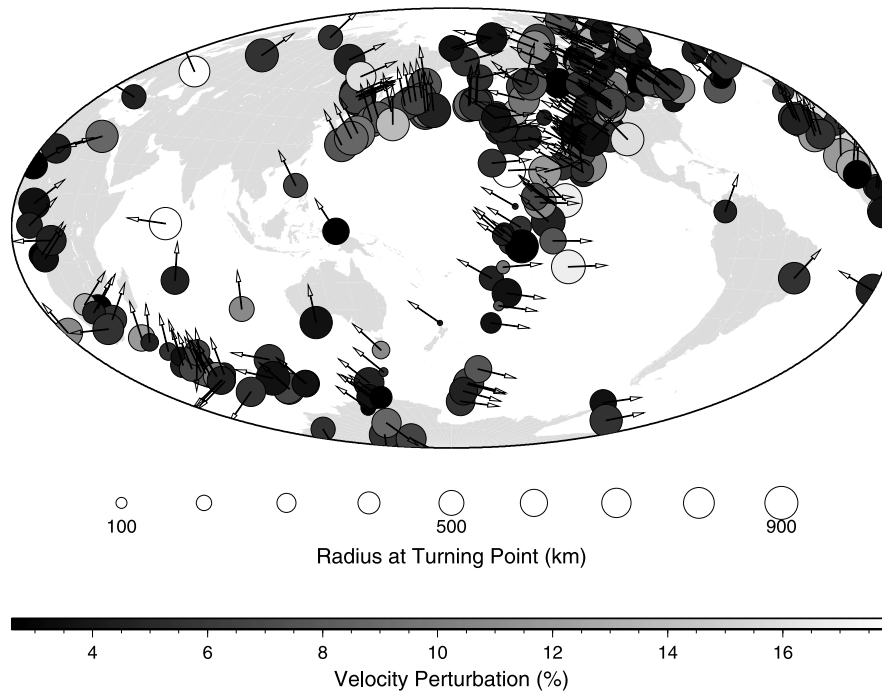
Figure 5. Global distribution of inverted velocity perturbation plotted at turning points of PKIKP ray paths. The arrow on each result is the ray direction at the turning point.

spatial coherence is seen in velocity perturbation (Figure 5), but less so in scale length (Figure 6). This suggests that the dispersive properties of scattering cannot always successfully remove the ambiguity in scale length as shown in Figure 4.

[16] The average scale length for all the 262 available results is 9.8 ± 2.4 km, and the average velocity perturbation is 8.4% ± 1.8% for the inner core from the center to about 1000 km radius. The magnitude of velocity perturbation is consistent with that estimated from the 1-D model, but the scale length is much larger. This difference may be due to fundamental differences in pulse broadening caused by 1-D versus 3-D heterogeneity or it may be due to the narrower searching band of scale lengths used in the 1-D study. The band of searched scale lengths may not have been broad enough to include the two
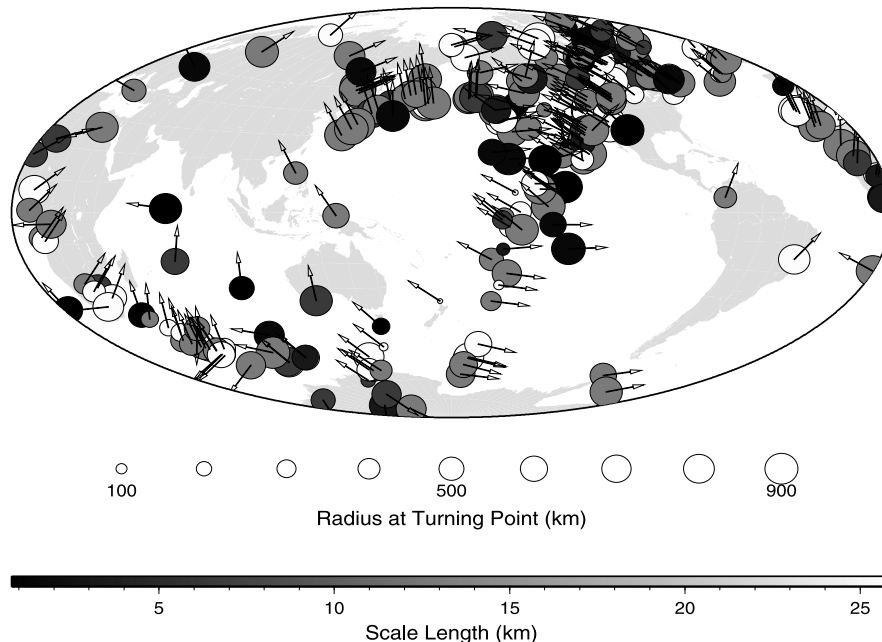

Figure 6. Global distribution of inverted scale length at turning points of PKIKP ray paths. The arrow on each result is the ray direction at the turning point.
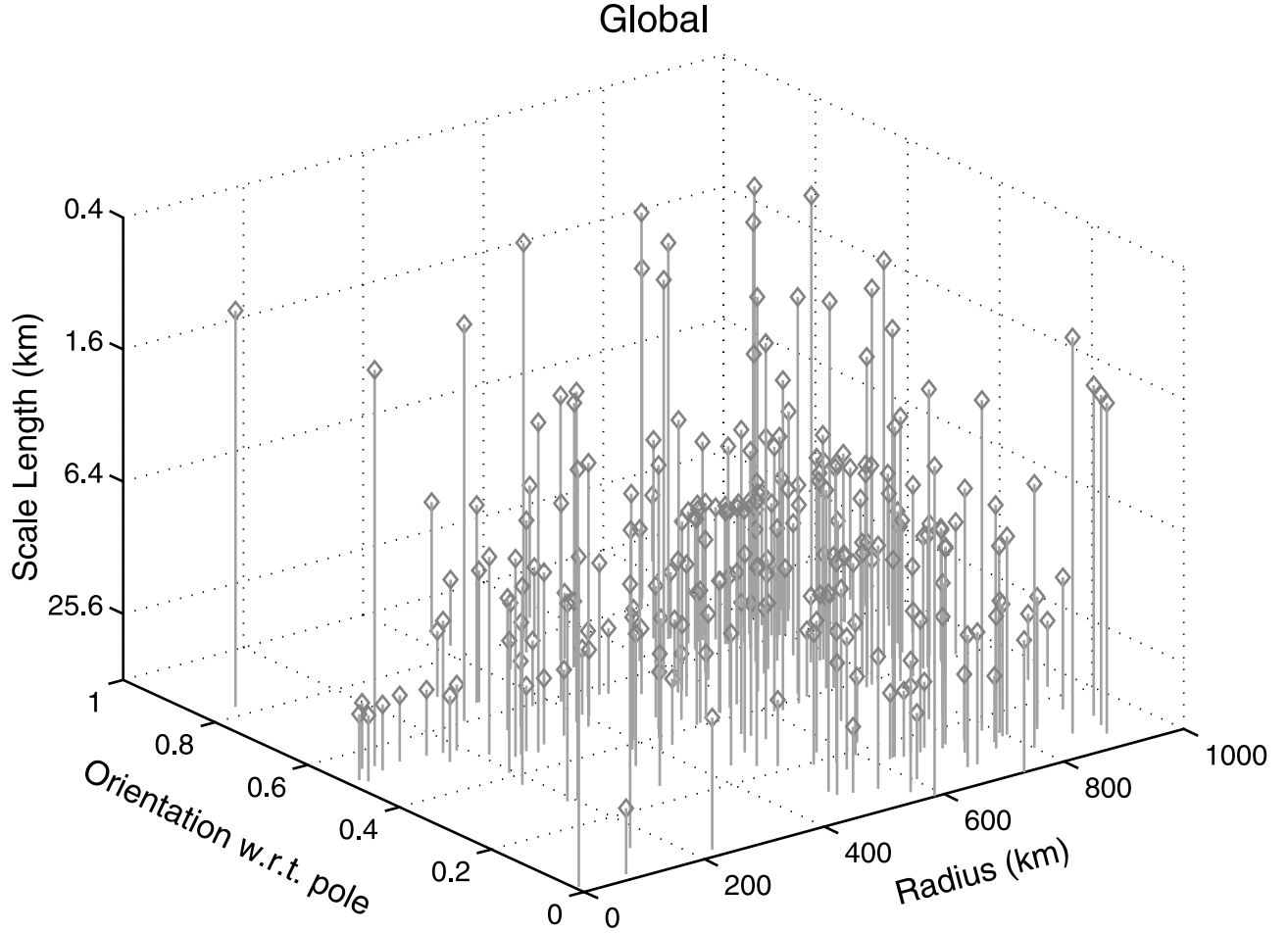
Global

Figure 7. Scale length as a function of radius and ray direction at the turning point of the PKIKP ray path, for (a) global and (b) North American data. Note the positive direction of scale length is downward. Depth dependence and anisotropy can be seen in North American data.

separate domains of scale lengths that can produce the same apparent attenuation as discussed in section 2.3 and shown in Figure 4.

[17] From the a stack of PKiKP coda waves, *Vidale and Earle* [2000] obtained a scale length of 2 km and elastic moduli variation of 1.2% across the outer 300 km of the inner core. Even though the investigated waveforms (backscattered versus forward scattered) and distance ranges (58−73° versus >150°) differ from our study, the large differences between our results and their results needs to be understood. Vidale and Earle assumed a viscoelastic Q of about 300 before generating the synthetic envelopes to fit backscattered coda envelope data, while we assume all attenuation to be caused by scattering. Thus their result for velocity perturbation can be considered to be a minimum estimate and our results a maximum estimate. Our results also represent averages over the whole inner core, while Vidale and Earle's time window of coda samples only the outer 300 km of the inner core. When we plot our results for scale length versus ray bottoming depth Figures 7a and 7b), we see evidence of small scale lengths (1−5 km), similar to Vidale and Earle's estimates, in the upper inner core beneath North America, which is the same region sampled by their study.

[18] Figures 8a and 8b plot the variation of the obtained velocity perturbation versus radius and ray direction at the turning point of PKIKP ray path for global data and North American data. The results show a clear depth-dependence for global and North American data. Small velocity perturbation tends to appear in the deep inner core, while high velocity perturbation tends to appear at the uppermost region of the inner core. For radii in the range of 600 ∼ 800 km, there seems to be a jump in the velocity perturbation. In the lower inner core, velocity perturbations are less than 6%, while in the upper inner core most results are greater than 8%. This behavior is not confined to North America. From Figure 5, we can see it exists globally. The narrow depth range of this transition might be consistent with a speculation of *Song and Helmberger* [1998] to explain coda complexities of long period PKIKP waves as the result of a sharp, laterally varying, boundary between a more intensely scattering and less intensely scattering region.

[19] The results for North America (Figure 8b) show clear anisotropy in addition to depth dependence. At ray directions close to the rotation axis at the ray turning point, the velocity perturbation tends to become large. This tendency, however, is relatively weak for the global data (Figure 8a), implying that the magnitude of the anisotropy is relatively
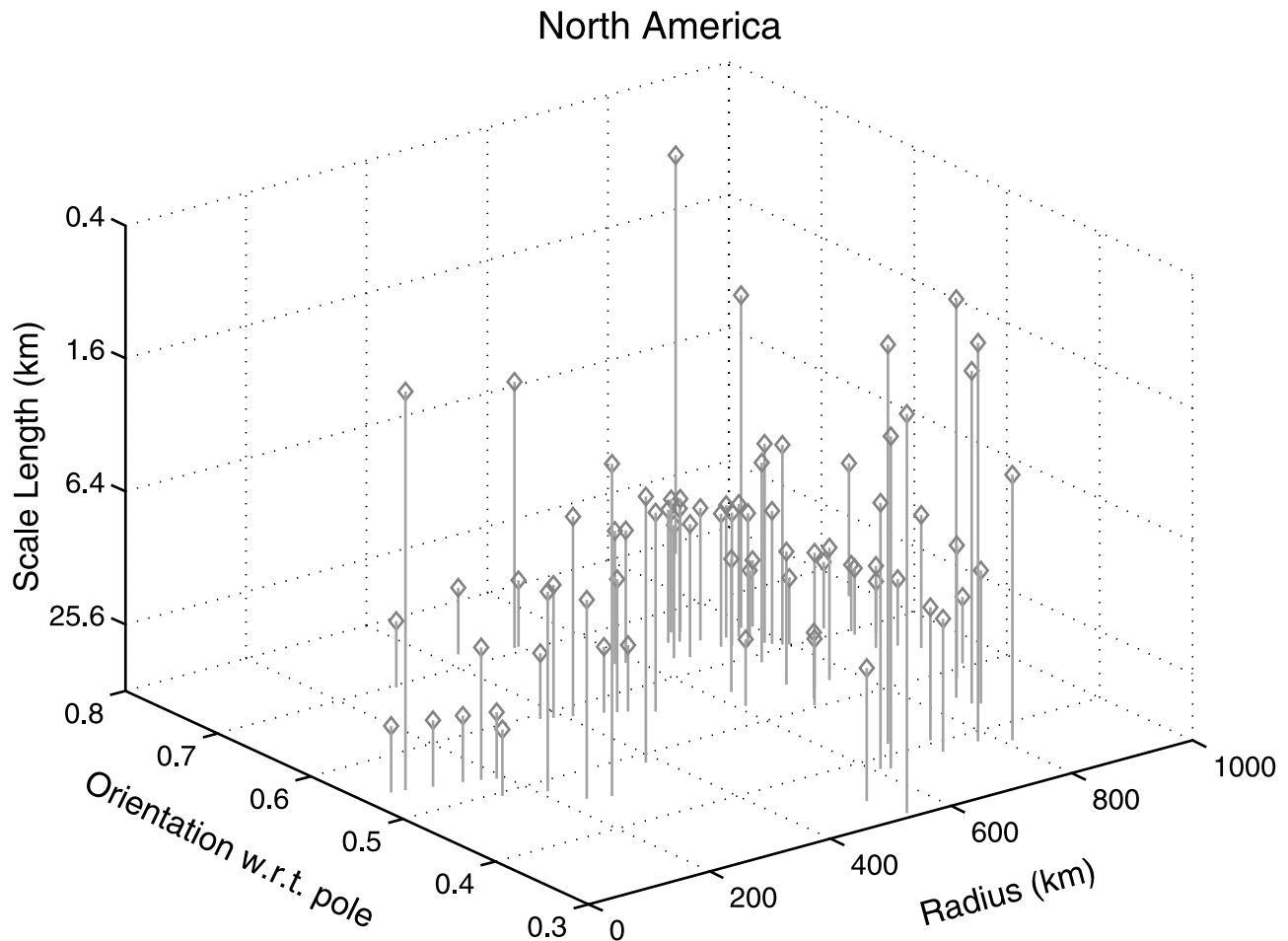
North America

Figure 7. (continued)

small compared to that of the lateral variations and depth dependence of attenuation. This suggests that only regionalized bins of data may be capable of resolving the anisotropy of attenuation.

[20] After obtaining the velocity perturbation and scale length, the corresponding apparent Q^{-1} at 1 Hz can be calculated. Its variation versus radius and ray direction at the turning point is shown in Figures 9a and 9b. The mean value of Q at 1 Hz is 259. The behavior with radius and turning point of inverted scattering attenuation generally agrees well with that of inverted viscoelastic attenuation (Figures 9a and 9b of paper 1). They are both depth-dependent and anisotropic and have significant differences in values for radii above and below 600 km. The scattering model predicts a much more abrupt rise in attenuation in the shallower inner core. At radii less than 600 km, Q^{-1} at 1 Hz is generally less than 0.003 and the mean value is 0.0025, while at radii larger than 600 km, values of Q^{-1} at 1 Hz increase significantly and are often larger than 0.006, having a mean value of 0.0048. Since there is no associated depth dependence of scale length in at least global data, we suggest that the pattern of depth dependent attenuation is primarily the result of changes in velocity perturbation. If the velocity perturbation is the result of changes in alignment of crystallographic axes across the boundaries of anisotropic crystals, then depth dependence could be sat-

isfied by an increasing degree of alignment of fast crystallographic axes with depth without significantly changing the size of crystals.

4. Discussion and Conclusions

4.1. Depth-Dependent and Anisotropic Attenuation: Its Meaning for Fabric

[21] Nearly all recent studies explain the observed elastic anisotropy from the preferred alignment of iron crystals with the fast direction nearly parallel to the rotation axis. At inner core temperature and pressure, iron is thought to have either a hcp (hexagonal close packed) or a fcc (face centered cubic) lattice. Many studies predict that the fastest P wave speed lies along the direction of either the ⟨001⟩ (c-axis) of hcp iron or the ⟨111⟩ of fcc iron [*Jeanloz*, 1990; *Stixrude and Cohen*, 1995; *Saxena et al.*, 1995]. Recent first-principles calculations by *Steinle-Neumann et al.* [2001], however, predict that the sense of anisotropy is reversed at high temperature in hcp iron, with P wave speed along the basal plane faster than along the c axis. The mechanisms to produce the preferred alignment of iron crystals vary from 1) growth of a single crystal [*Stixrude and Cohen*, 1995]; 2) deformation-induced texturing during thermal convection [*Jeanloz and Wenk*, 1988; *Wenk et al.*, 1988, 2000]; 3) growth in a strong magnetic field [*Kanato*, 1993; *McSwee-*
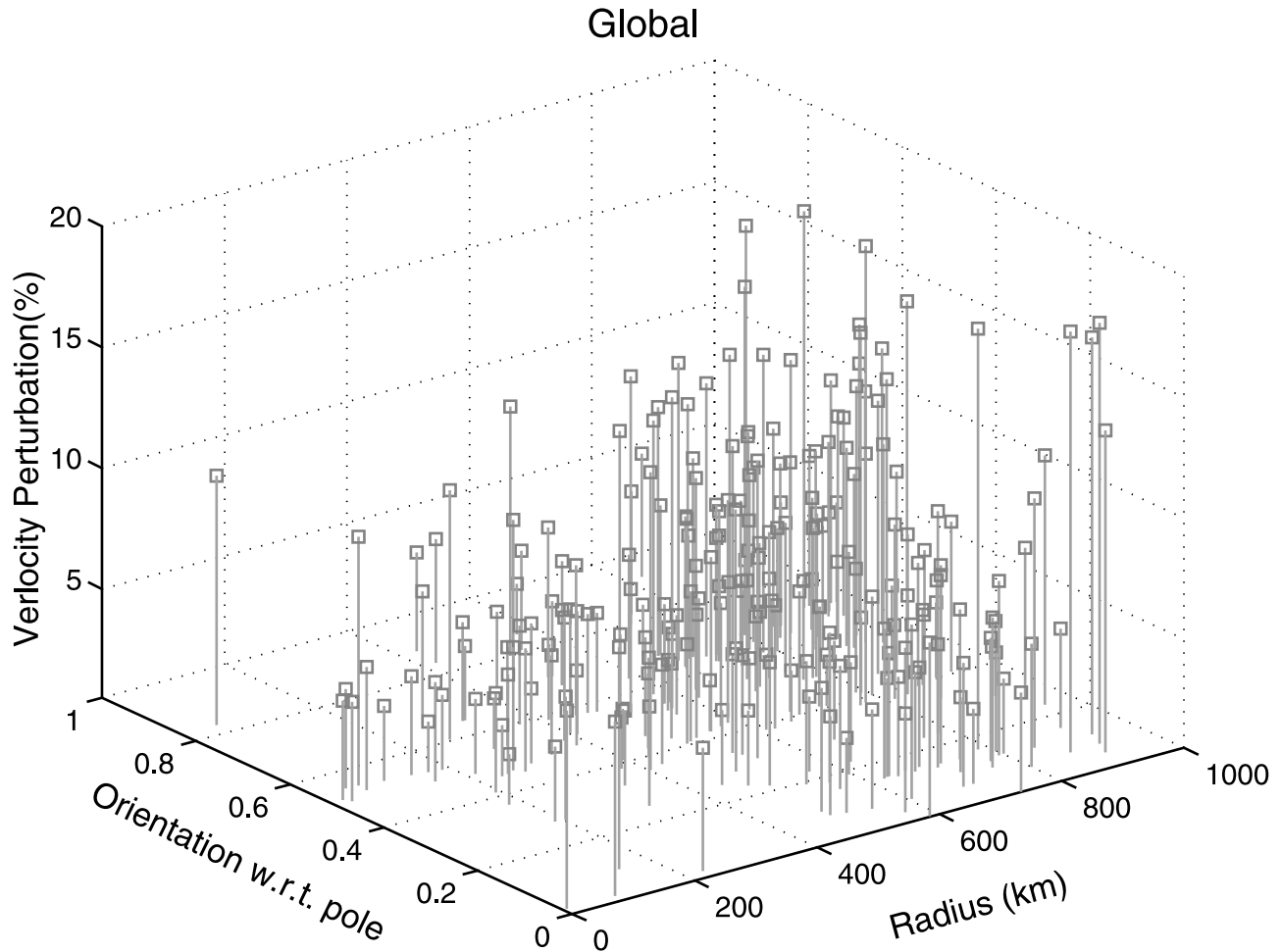
Figure 8. Velocity perturbation as a function of radius and ray direction at the turning point of the PKIKP ray path for (a) global and (b) North American data. Strong depth dependence can be observed in both data sets, while anisotropy can be seen in the North American data set.

ney et al., 1997]; 4) solidification texturing of crystals aligned by heat flow [Bergman, 1997]; and 5) growth in a latitude-dependent stress field [Yoshida et al., 1996; Karato, 1999; Buffett and Wenk, 2001]. The existence of the inner core as a gigantic single crystal model could not easily explain the depth dependence of elastic anisotropy observed in seismic data [Vinnik et al., 1994; Shearer, 1994; Su and Dziewonski, 1995; Song, 1996]. It is also no longer necessary to invoke a single crystal to explain the magnitude of the observed seismic anisotropy [Steinle-Neumann et al., 2001]. Yoshida et al [1996] rule out alignment by convection due to the high thermal conductivity of and probable lack of significant radiogenic heat in the inner core. They also rule out alignment by growth in a magnetic field due to its prediction of increasing rather than decreasing anisotropy near the ICB. Hence, we will just discuss two possibilities here: growth and solidification texturing by either heat flow or latitude-dependent stress.

4.1.1. Solidification Texturing by Heat Flow

[22] Without considering the effects of flow and deformation, Bergman [1997] has described a solidification texturing resulting from a cylindrical heat flow driven by the tangent cylinders of outer core convection cells. Extraction of heat primarily perpendicular to the rotation axis will cause growth of dendrites elongated in the cylindrically radial direction (Figure 10). For the hcp phase, the solidification-texturing mechanism Bergman predicts that the $\langle 210 \rangle$ crystal axes will lie in the cylindrically radial direction, with the $\langle 001 \rangle$, $\langle 010 \rangle$ axes lying in any perpendicular direction (no preferential alignment). This model successfully explains an attenuation anisotropy, with attenuation greater for P waves propagating parallel to the rotation axis. The columnar crystals elongated in the cylindrically radial direction may be responsible for an attenuation anisotropy, with a greater attenuation for P waves propagating nearly parallel to the rotation axis. For a given turning radius, these polar P waves generally will cross more crystal boundaries than will equatorial waves propagating perpendicular to the rotation axis. Scattering attenuation occurs due to the velocity contrast between the differently oriented $\langle 001 \rangle$ and $\langle 010 \rangle$ axes across the crystal boundaries. Since many more crystal boundaries are crossed per unit distance travel in the polar direction than in other directions, the aggregate scale length inferred from pulse broadening should be relatively smaller in the polar directions. For waves propagating in equatorial directions, higher attenuation and smaller apparent scale length will be inferred from shallow penetrating rays, but the attenuation will decrease and the apparent scale length
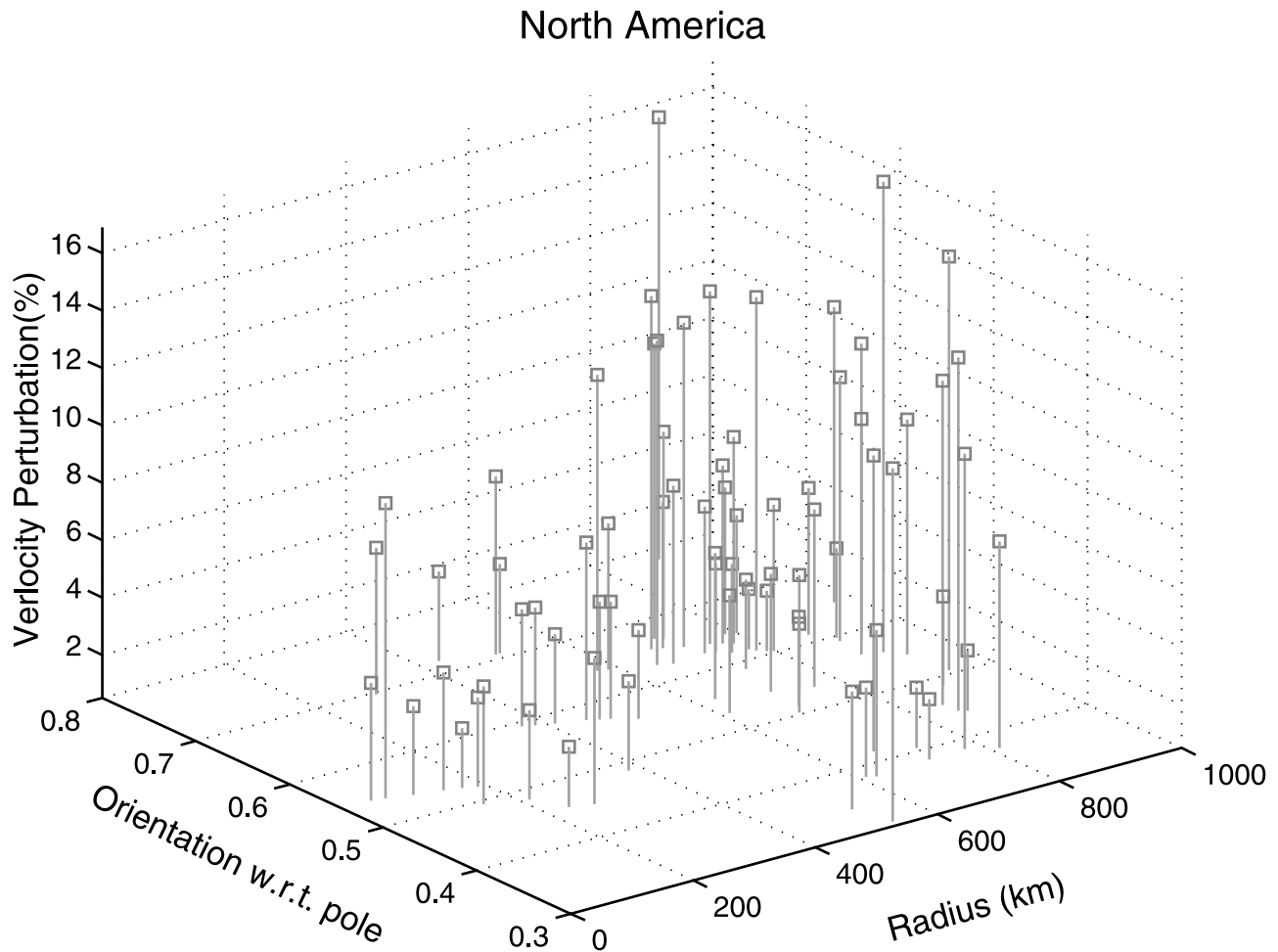
Figure 8. (continued)

will increase for more deeply penetrating rays. This is just what we observed in Figure 7b for North American data, in which the scale length is small for rays having either a shallow turning depth or a propagation direction parallel to the rotation axis. Thus this model at least partially explains the depth-dependent attenuation we observe. For polar waves propagating parallel to the rotation axis, however, shallow rays will cross almost the same number of crystal boundaries per unit distance as the deeper rays. Thus, *depth-independent* attenuation will be predicted for the case of rays propagating in polar planes, and *depth-dependent* attenuation will be predicted for rays propagating in the equatorial planes. This is inconsistent with observations (Figure 9), which find depth-dependent attenuation along *both* polar and equatorial directions. If the predictions of *Steinle-Neumann et al.* [2001] are accepted, in which the ⟨001⟩ (c axis) is no longer the fast axis as originally assumed by *Bergman* [1997], then the predicted elastic anisotropy of the Bergman fabric will also be inconsistent with observations.

4.1.2. Texturing by a Latitude-Dependent Stress Field

[23] A latitude-dependent stress field may originate by any one effect or combination of effects, including aspherical growth of the inner core [*Yoshida et al.*, 1996], gravitational coupling with the mantle [*Buffett*, 1997], or Maxwell stresses created by the Earth's magnetic field [*Karato*, 1999;

Buffett and Wenk, 2001]. Regardless of the origin of a latitude-dependent stress field and the mechanisms of deformation and possible recrystallization, all of the flow-textured models predict a layer near the ICB in which the preferred alignments are small. This prediction agrees with observations of weak anisotropy in the uppermost inner core [e.g., *Song and Helmberger*, 1995]. In the shallow inner core, where with the solidification is occurring, crystals will be relatively too young to reach to their final orientation state under the changing stress state. In this region, the greater disorder of crystals having the high intrinsic anisotropy (12%) predicted by *Steinle-Neumann et al.* [2001] will result in a greater amount of scattering attenuation. In agreement with observations, the attenuation will exhibit strong depth dependence along both equatorial and polar paths. With increasing time and depth in the inner core, a final state of alignment will be achieved, depending on the dominant direction of flow. For a polar dominated flow, *Steinle-Neumann et al.* [2001] predict that the easiest glide planes (basal planes of hcp iron) will tend to align with the rotation axis. Their predicted elastic constants require that only about 1/3 of the basal planes of hcp iron be aligned with the rotation axis in the deeper region of the inner core to satisfy the observed anisotropy of PKIKP travel times.
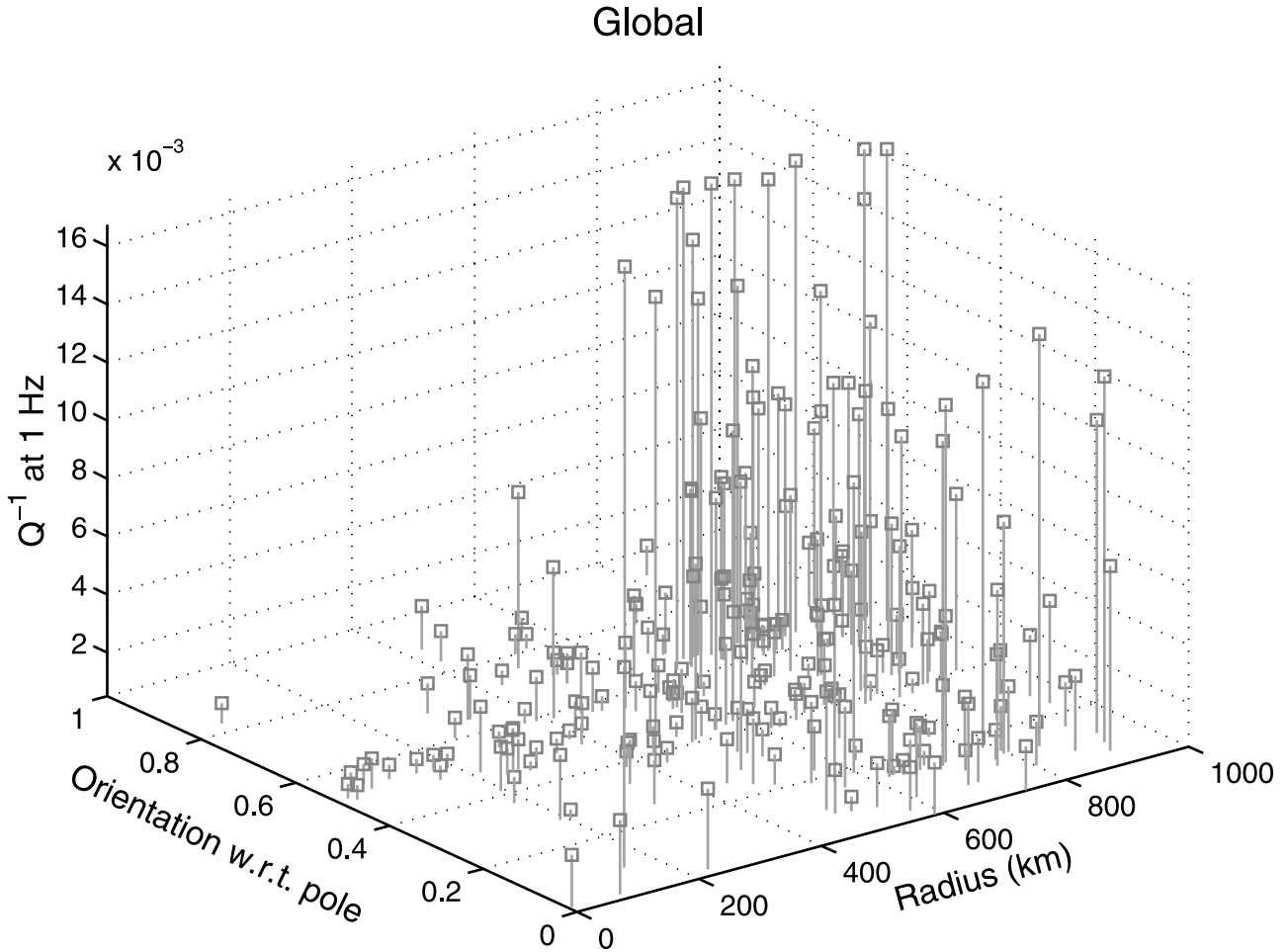
Figure 9. Q^{-1} (1 Hz) as a function of radius and ray direction at the turning point of the PKIKP ray path for (a) global and (b) North American data. A steep rise at radius of 600 km is visible in both sets of data.

4.1.3. Combining Constraints

[24] A more complex fabric may exist in a the shallow inner core, where the effects of crystal growth in the cylindrical radial direction combine with a flow field driven by a latitude-dependent stress field. In this region, deformation and recrystallization may not have completely finished due to the short time history after its solidification. Crystal orientation will generally be more random in the shallower inner core than in the deeper inner core, resulting in high scattering attenuation due to the large velocity perturbations across grain boundaries in most directions. The effects of radial growth on orienting the $\langle 210 \rangle$ axes in the shallowest regions of the inner core may contribute to a higher level of scattering attenuation along polar paths. The magnitude of intrinsic elastic anisotropy of each grain, and consequently the size of velocity discontinuities at grain boundaries, might also be enhanced near the ICB by the higher homologous temperature in this region [*Fisher and Renken*, 1964].

[25] In the deep inner core, solidification, deformation and recrystallization have completely finished. In this region, flow has aligned crystals along their fast direction, independent of whether the fast direction is the basal plane direction or the c axis. To reduce the effects of scattering along both polar and equatorial paths in the deep inner core, either the intensity of intrinsic anisotropy must decrease or the alignment is such as to reduce the effective velocity contrasts across crystal boundaries.

[26] To account for the relatively sharp jump in scattering attenuation near 600 km radius (Figure 9), a strong effective velocity change may be required by composite medium theories. Indeed, *Song and Helmberger* [1998] have suggested the possibility of and reviewed evidence for either a discontinuity or a rapid change in elastic moduli in a laterally varying transition region between the upper and lower inner core.

[27] One possibility for explaining the observed sharpness in the fabric transition may be the existence of a partially molten zone [*Fearn et al.*, 1981; *Loper and Fearn*, 1983]. Metallurgic experiments [e.g., *Copley et al.*, 1970] suggest that this mushy zone could exist between the liquid outer core and solid inner core. The dendrites and fluid inclusions in the mushy zone can produce additional velocity perturbations
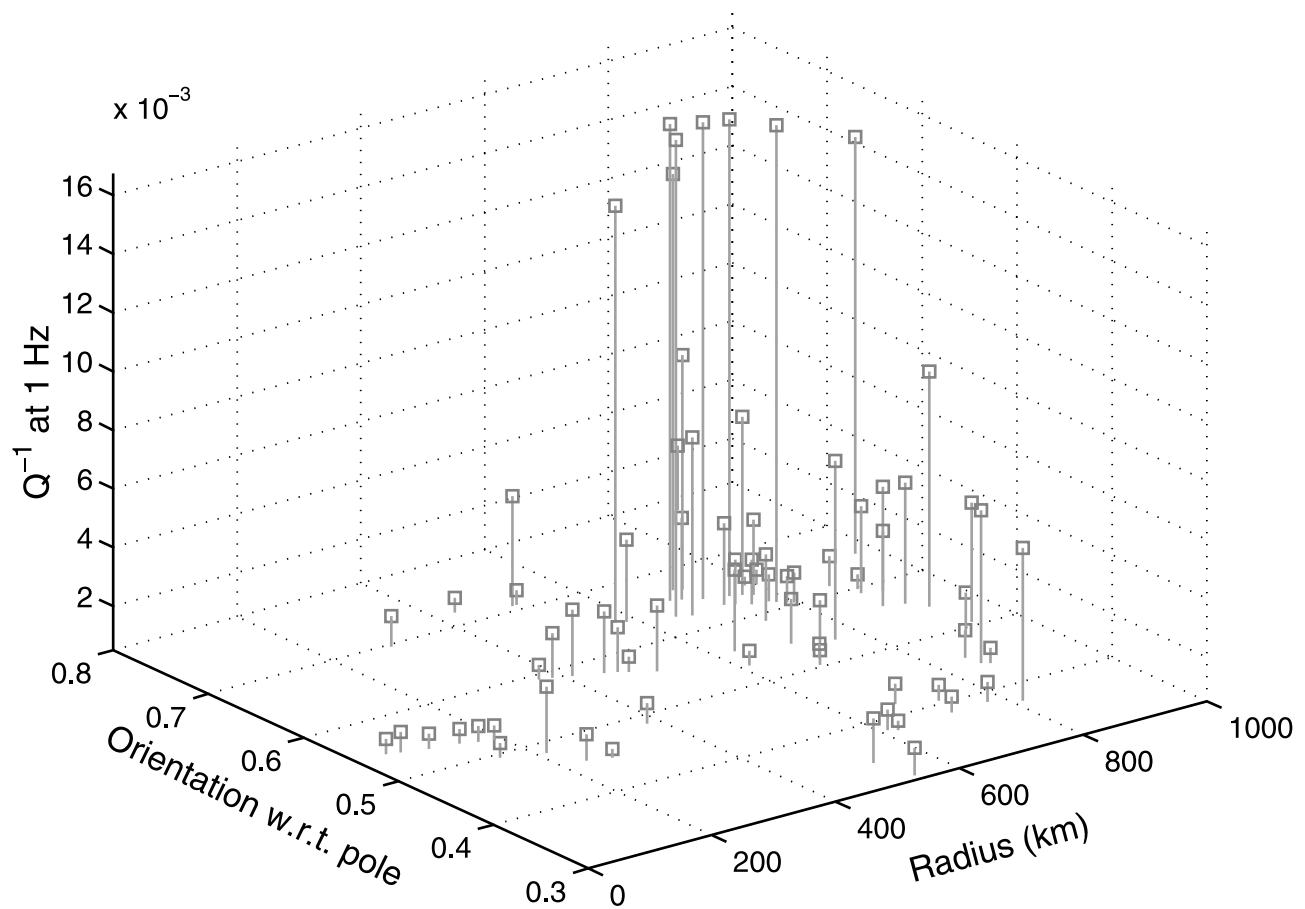
North America

Figure 9. (continued)

and scattering as well as viscoelastic attenuation [*Cormier, 1981; Singh et al.*, 2000]. An apparent discontinuity in elastic moduli might exist somewhere near but not necessarily coincident with the depth in which the last amount of liquid vanishes. Similar to the suggestion by *Herrmann and Bernabe* [2001] for the nature of the upper mantle phase transitions, there might exist a critical point near the bottom of the mushy zone where at least the first depth derivative of the composite elastic moduli is discontinuous. Whether such a mushy zone could extend 600 km or deeper into the inner core, however, may be doubtful. *Fearn et al.* [1981] suggest that a mushy zone may extend throughout the entire inner core, but *Sumita et al.* [1995, 1996] argue that the melt would be less dense than its surrounding solid matrix and would be buoyantly squeezed out of the inner core.

[28] It would seem that the alternative process of solidification-texturing and recrystallization with insignificant amounts of partial melt would occur smoothly with depth and be incapable of producing such a sharp transition in fabric. Like partial melt, however, it may be possible to induce a sharp transition in fabric properties and the long-wavelength composite modulus when a critical point has been reached in the concentration of a particular orientation of iron crystals.

[29] In summary, the depth dependence and anisotropy of attenuation in the inner core can be explained by the

combination of a growth and solidification model with a possible mushy zone in the upper half of inner core. An increase in the preferred alignments of individual iron crystals with depth in inner core can predict both the global variation of PKIKP pulse widths as well as the observed depth dependence of the elastic anisotropy of the composite elastic moduli. We thus argue that scattering by a heterogeneous fabric would be the predominant contribution to attenuation in the inner core in the frequency band of body waves. Figure 11 illustrates a possible the fabric to account for the depth-dependent attenuation observed in this study. In the deep part of the inner core, the iron crystals have been perfectly aligned under solidification texturing and isostatic adjustment in the history of its formation. The near perfect alignment accounts for the strong elastic anisotropy and small attenuation in the deeper part of inner core. In the upper part of the inner core, the alignment of iron crystals is incomplete. A mushy zone may exist in the upper inner core, contributing to an abrupt jump of attenuation between the lower and upper inner core. As discussed in section 4.2 of this paper, a mushy zone may also be required to account for observations of differential rotation of the inner core.

[30] A model having a sharp depth transition in fabric is similar to one proposed by *Song and Helmberger* [1998] to explain the pulse-broadening of long-period PKIKP waveforms and complexity observed in some short-period
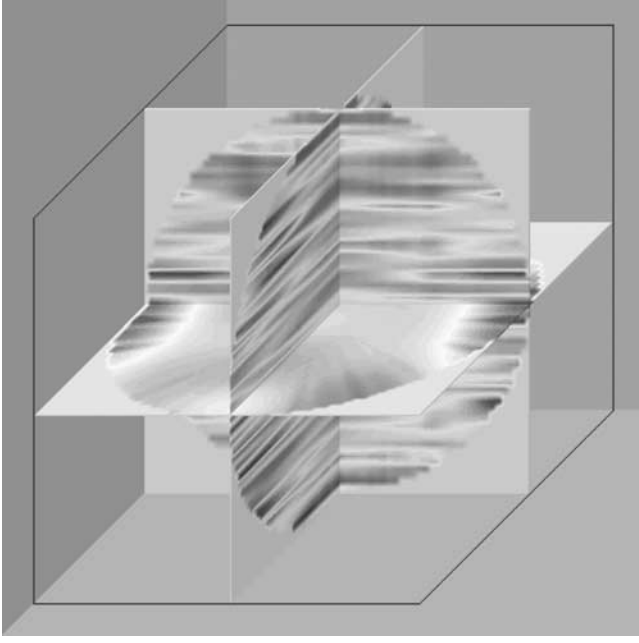
Figure 10. Polar and equatorial cross sections through a model of inner core texture based on *Bergman*'s [1997] model of inner core solidification. For visibility, spatial scales of variations are exaggerated by a factor of 10 or more compared to those inferred from inverted PKIKP waveforms.

PKIKP waveforms. They suggest a sharp P velocity jump of $3.5\% \sim 5\%$ at $200 \sim 300$ km from ICB. Our interpretation, however, is simply a jump or rapid transition in the statistical parameters describing velocity perturbation rather than in the velocity itself. Observations of long period pulse broadening can be explained by scattering in this layer (e.g., Figure 3b). The waveform complexities seen in short period data could also be explained by an increase in scale lengths of iron crystals under the mushy zone. In fact, we see evidence that at 400 km beneath ICB, the scale length may increase to several ten's of kilometers (Figure 7b) as suggested in Song and Helmberger's paper.

4.2. Implications of Scale Length Distribution

[31] The scale lengths or grains sizes in the inner core have implications for the viscosity of the inner core. The viscosity affects the gravitational coupling of the inner core to mass inhomogeneities in the mantle [*Buffett*, 1997]. Using Buffett's upper viscosity bound of 10^{16} Pa-s for gravitational coupling, *Bergman* [1998] estimates that grain sizes higher than 5 mm will prevent differential rotation rates as high as the $1-3°$ yr^{-1} suggested by secular variations of PKIKP travel times [*Song and Richards*, 1996; *Su et al.*, 1996]. Assuming that differential rotation rates even as low as $0.1-0.2°$ yr^{-1} [*Vidale et al.*, 2000] withstand continued scrutiny, our >1 km estimates of scale length suggest that a mechanism other than grain boundary diffusion must be invoked to sufficiently lower the viscosity of the inner core to allow its differential rotation. *Bergman* [1998] lists the existence of a low viscosity mushy zone in the upper inner core as one possible mechanism. Another mechanism could be the enhancement of dislocation glide

along the basal planes of hcp iron at high temperature [*Wenk et al.*, 2000a, 2000b; *Steinle-Neumann et al.*, 2001].

5. Reconciliation With Free Oscillation Measurements

[32] Across the complete frequency band of seismic measurements, inner core attenuation can be explained by a combination of viscoelastic and scattering effects. Since the PKiKP coda wave modeling of *Vidale and Earle* [2000] have clearly established the existence of a scattering component to inner core attenuation, future studies of inner core attenuation should attempt to carefully examine the trade-offs between viscoelastic and scattering attenuation for observations body wave band of frequencies. Nonetheless, some bounds on the relative contributions of viscoelasticity and scattering can be established from our current study as well previous studies. Expressed quantitatively, the total attenuation $Q^{-1} = Q_A^{-1} + Q_S^{-1}$, where the first term accounts for viscoelastic attenuation and second one for scattering attenuation. The viscoelastic attenuation, Q_A^{-1}, of a P wave can be also expressed as a linear combination of pure shear attenuation Q_μ^{-1} and pure bulk attenuation Q_κ^{-1}:

$$Q_A^{-1} = \frac{4}{3}(V_S/V_P)^2 Q_\mu^{-1} + \left[1 - \frac{4}{3}(V_S/V_P)^2\right]Q_\kappa^{-1} \quad (4)$$

[*Anderson and Hart*, 1978], where V_S and V_P are S- and P wave velocity respectively. *Widmer et al.* [1991] found from free oscillation data with frequencies in the band of $0.001 \sim 0.007$ Hz that the shear attenuation factor Q_μ in the inner core is 110. If the shear attenuation is due to a viscoelastic mechanism extrapolated at constant strength into the band of body waves, it will contribute only 0.00128 to the total Q^{-1} [*Cormier et al.*, 1998]. This value is much less than the
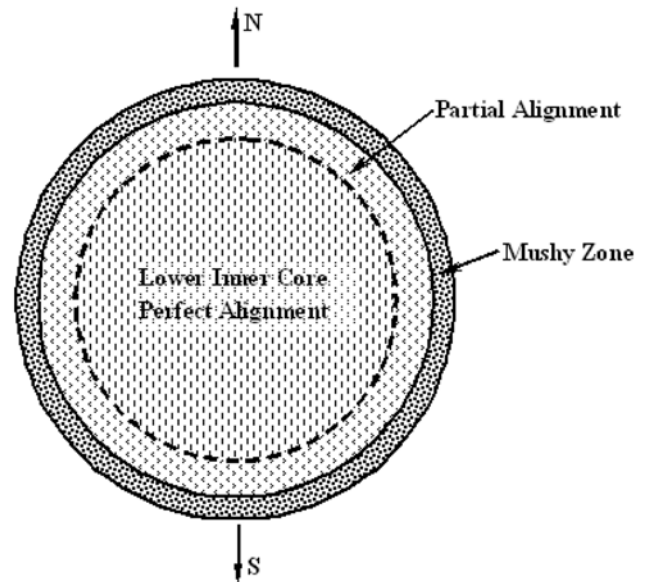

Figure 11. A schematic inner core structure to account for the depth-dependent attenuation observed in this study. This structure will account for the strong elastic anisotropy and small attenuation in the deep part of the inner core.

values of Q^{-1} of 0.0025 $\sim$ 0.005 commonly found in this and all other preceding studies of body wave attenuation. The additional P attenuation in the body wave band can be reconciled by either 1) frequency-dependent viscoelastic shear attenuation, 2) scattering attenuation in the high frequency band of body waves, or 3) viscoelastic bulk attenuation. If shear viscoelastic attenuation increases with frequency at its fastest allowable rate (proportional to frequency) into the higher frequency band of body waves (0.02 to 2 Hz), it can explain the total attenuation, but it would require a physically unrealistic modulus defect in shear.

[33]   Alternatively, the second or third possibilities (either viscoelastic bulk or scattering attenuation) is an easy way to reconcile the free oscillation measurements. As suggested by *Loper and Fearn* [1983], if there is a partially molten zone in upper inner core, the bulk attenuation induced by thermal and material diffusion will be considerable. Moreover if the volume fraction of liquid is as large as 0.5, the bulk attenuation itself can be responsible for the observed high attenuation at body wave frequencies in the upper inner core. As we noted previously, however, a large amount of liquid is likely to be buoyantly expelled into the outer core, with the remaining volume of liquid expected to be very small. Scattering attenuation in the inner core is consistent both with the backscattered PKiKP coda observed by *Vidale and Earle* [2000] and with the forward scattering analysis of PKIKP pulse broadening of this study. A comparison of Figure 2 with Vidale and Earle's estimates of velocity perturbation (1.2%) and scale length (2 km), which we take as lower bounds to the true values, suggests that at least 25% of the observed attenuation in the body wave band can be explained by scattering. Elastic anisotropy, its depth dependence, and dispersion with frequency, and the depth dependence, and anisotropy of observed attenuation agree with that predicted by the scale lengths and velocity perturbations of disordered, elastically anisotropic iron crystals. We thus suggest that scattering attenuation is not a small fraction but rather the predominant mechanism of attenuation in the inner core in the 0.02 to 2 Hz frequency band.

References

Anderson, D. L., and R. S. Hart, Q of the Earth, *J. Geophys. Res.*, *83*, 5869–5882, 1978.

Bergman, M. I., Measurements of elastic anisotropy due to solidification texturing and the implications for the Earth's inner core, *Nature*, *339*, 60–63, 1997.

Bergman, M. I., Estimates of Earth's inner core grain size, *Geophys. Res. Lett.*, *25*, 1593–1596, 1998.

Berryman, J. G., Long-wavelength propagation in composite elastic media, 1, Spherical inclusions, *J. Acoust. Soc. Am.*, *68*, 1809–1819, 1980.

Buffett, B. A., Geodynamic estimates of the viscosity of the Earth's inner core, *Nature*, *388*, 571–573, 1997.

Buffett, B. A., and H.-R. Wenk, Texturing of the Earth's inner core by Maxwell stresses, *Nature*, *413*, 60–63, 2001.

Copley, S. M., A. F. Giamei, S. M. Johnson, and M. F. Hornbecker, The origin of freckles in unidirectionally solidified castings, *Metall. Trans.*, *1*, 2193–2204, 1970.

Cormier, V. F., Short-period PKP phase and the anelastic mechanism of the inner core, *Phys. Earth Planet. Inter.*, *24*, 291–301, 1981.

Cormier, V. F., X. Li, and G. L. Choy, Seismic attenuation of the inner core: Viscoelastic or stratigraphic?, *Geophys. Res. Lett.*, *25*, 4019–4022, 1998.

Fearn, D. R., D. E. Loper, and P. H. Roberts, Structure of the Earth's inner core, *Nature*, *292*, 232–233, 1981.

Fisher, E. S., and C. J. Renken, Single crystal elastic moduli and the hcp-bcc transformation in Ti, Zr, and Hf, *Phys. Rev.*, *135*, A428–A494, 1964.

Herrmann, F., and Y. Bernabe, Upper mantle seismic discontinuities predicted by site percolation (abstract), *Eos Trans. AGU*, *82*(47), Fall Meet. Suppl., Abstract S42B-0628, 2001.

Jeanloz, R., The nature of Earth's core, *Annu. Rev. Earth Planet. Sci.*, *18*, 357–386, 1990.

Jeanloz, R., and H. R. Wenk, Convection and anisotropy of the inner core, *Geophys. Res. Lett.*, *15*, 72–75, 1988.

Kaelin, B., and L. R. Johnson, Dynamic composite elastic medium theory, 2, Three-dimensional media, *J. Appl. Phys.*, *84*, 5458–5468, 1998.

Kanato, S., Inner core anisotropy how to magnetic field-induced preferred orientation of iron, *Science*, *262*, 1708–1711, 1993.

Karato, S., Seismic anisotropy of Earth's inner core resulting from flow induced by Maxwell stresses, *Nature*, *402*, 871–873, 1999.

Korneev, V. A., and L. R. Johnson, Scattering of elastic waves by a spherical inclusion, 1, Theory and numerical results, *Geophys. J. Int.*, *115*, 230–250, 1993a.

Korneev, V. A., and L. R. Johnson, Scattering of elastic waves by a spherical inclusion, 2, Limitations of asymptotic solutions, *Geophys. J. Int.*, *115*, 251–263, 1993b.

Korneev, V. A., and L. R. Johnson, Scattering of P and S waves by a spherically symmetric inclusion, *Pure Appl. Geophys.*, *147*, 675–718, 1996.

Kuster, G. T., and M. N. Toksoz, Velocity and attenuation of seismic waves in two-phase media, 1, Theoretical formulations, *Geophysics*, *38*, 587–606, 1974.

Li, X., and V. F. Cormier, Frequency-dependent seismic attenuation in the inner core, 1, A viscoelastic interpretation, *J. Geophys. Res.*, *107*, doi:10.1029/2002JB001795, in press, 2002.

Loper, D. E., and D. R. Fearn, A seismic model of a partially molten inner core, *J. Geophys. Res.*, *88*, 1235–1242, 1983.

McSweeney, T. J., K. C. Creader, and R. T. Merrill, Depth extent of inner-core seismic anisotropy and implications for geomagnetism, *Phys. Earth Planet. Inter.*, *101*, 131–156, 1997.

Richards, P. G., and W. Menke, The apparent attenuation of a scattering medium, *Bull. Seismol. Soc. Am.*, *73*, 1005–1021, 1983.

Saxena, S. K., L. S. Dubrovinsky, P. Haggkvist, Y. Cerenius, G. Shen, and H. K. Mao, Synchrotron X-ray study of iron at high pressure and temperature, implications for the Earth's core, *Science*, *269*, 1703–1704, 1995.

Shearer, P. M., Constraints on inner core anisotropy from PKP(DF) travel times, *J. Geophys. Res.*, *99*, 19,647–19,659, 1994.

Singh, S. C., M. A. J. Taylor, and J. P. Montagner, On the presence of liquid in earth's inner core, *Science*, *287*, 2471–2474, 2000.

Song, X. D., Anisotropy in central part of inner core, *J. Geophys. Res.*, *101*, 16,089–16,097, 1996.

Song, X. D., and D. V. Helmberger, Depth dependence of anisotropy of Earth's inner core, *J. Geophys. Res.*, *100*, 9805–9816, 1995.

Song, X. D., and D. V. Helmberger, Seismic evidence for an inner core transition zone, *Science*, *282*, 924–927, 1998.

Song, X. D., and P. G. Richards, Seismological evidence for the rotation of the Earth's inner ore, *Nature*, *382*, 221–224, 1996.

Steinle-Neumann, G., L. Stixrude, R. E. Cohen, and O. Gulseren, Elasticity of iron at the temperature of the Earth's inner core, *Nature*, *413*, 57–60, 2001.

Stixrude, L., and R. E. Cohen, High-pressure elasticity of iron and anisotropy of Earth's inner core, *Science*, *267*, 1972–1975, 1995.

Su, W. J., and A. M. Dziewonski, Inner core anisotropy in the three dimensions, *J. Geophys. Res.*, *100*, 9831–9852, 1995.

Su, W. J., A. M. Dziewonski, and R. Jeanloz, Planet within a planet: Rotation of the inner core of the Earth, *Science*, *274*, 1883–1887, 1996.

Sumita, I., S. Yoshida, Y. Hamano, and M. Kumazawa, A model for the structural evolution of the Earth's core and its relation to the observations, in *The Earth's Central Part: Its structure and Dynamics*, edited by T. Yukutake, pp. 231–261, Terra Sci., Tokyo, 1995.

Sumita, I., S. Yoshida, M. Kumazawa, and Y. Hamano, A model for sedimentary compaction of a viscous medium and its application to inner-core growth, *Geophys. J. Int.*, *124*, 502–524, 1996.

Vidale, J. E., and P. S. Earle, Fine-scale heterogeneity in the Earth's inner core, *Nature*, *404*, 273–275, 2000.

Vidale, J. E., D. A. Dodge, and P. S. Earle, Slow differential rotation of the Earth's inner core indicated by temporal changes in scattering, *Nature*, *405*, 445–448, 2000.

Vinnik, L., B. Romanowicz, and L. Breger, Anisotropy in the center of the Earth, *Geophys. Res. Lett.*, *21*, 1671–1674, 1994.

Wenk, H.-R., T. Takeshita, R. Jeanloz, and G. C. Johnson, Development of texture and elastic anisotropy during deformation of hcp metals, *Geophys. Res. Lett.*, *15*, 76–79, 1988.

Wenk, H.-R., J. R. Baumgardner, R. A. Lebensohn, and C. N. Tome, A convection model to explain anisotropy of the inner core, *J. Geophys. Res.*, *105*, 5663–5677, 2000a.

Wenk, H.-R., S. Matthies, R. J. Hemley, H. K. Mao, and J. Shu, The plastic deformation of iron at pressures of the Earth's inner core, *Nature*, *405*, 1044–1047, 2000b.

Widmer, R., G. Masters, and F. Gilbert, Spherically symmetric attenuation within the Earth from normal mode data, *Geophys. J. Int.*, *104*, 541–553, 1991.

Wu, R. S., and K. Aki (Eds.), *Scattering and Attenuation of Seismic Waves, vol. 1* (special issues of *Pure Appl. Geophys.*), Birkhäuser Boston, Cambridge, Mass., 1988.

Yoshida, S., I. Sumita, and M. Kumazawa, Growth model of the inner core coupled with the outer core dynamics and the resulting elastic anisotropy, *J. Geophys. Res.*, *101*, 28,085–28,103, 1996.

———————————

V. F. Cormier, Department of Geology and Geophysics, University of Connecticut, 354 Mansfield Road, Room 207, Storrs, CT 06269-2045, USA. (cormier@geol.uconn.edu)

X. Li, Earth Resources Laboratory, Department of Earth, Atmospheric, and Planetary Science, Massachusetts Institute of Technology, 42 Carleton Street, Cambridge, MA 02142, USA. (xuli@erl.mit.edu)